Articles

Crystal Structure of L-Arginine:Inosamine-Phosphate Amidinotransferase StrB1 from *Streptomyces griseus*: An Enzyme Involved in Streptomycin Biosynthesis‡

Erich Fritsche,*,§ Andreas Bergner,§ Andreas Humm,§ Wolfgang Piepersberg,|| and Robert Huber§

Max-Planck-Institut für Biochemie, Abteilung für Strukturforschung, Am Klopferspitz 18a, D-82152 Martinsried, Germany, and Bergische Universität GH, Chemische Mikrobiologie, Gaussstrasse 20, D-42097 Wuppertal, Germany

Received August 12, 1998; Revised Manuscript Received September 28, 1998

ABSTRACT: Inosamine-phosphate amidinotransferases catalyze two nonconsecutive transamidination reactions in the biosynthesis of the streptomycin family of antibiotics. L-Arginine:inosamine-phosphate amidinotransferase StrB1 from *Streptomyces griseus* (StrB1) was cloned as an N-terminal hexa-histidine fusion protein, purified by affinity chromatography, and crystallized, and its crystal structure was solved by Patterson search methods at 3.1 Å resolution. The structure is composed of five $\beta\beta\alpha\beta$-modules which are arranged circularly into a pseudo-5-fold symmetric particle. The three-dimensional structure is closely related to the structure of human L-arginine:glycine amidinotransferase (AT), but five loops (the 40-, 170-, 220-, 250-, and 270-loop) are organized very differently. The major changes are found in loops around the active site which open the narrow active site channel of AT to form an open and solvent-exposed cavity. In particular, module II of StrB1 is AT-like but lacks a 10-residue α-helix in the 170-loop. The concomitant reorganization of neighboring surface loops that surround the active site, i.e., the 40-loop and the 270-loop, results in an arrangement of loops which allows an unrestricted access of substrates to the cavity. However, the residues which are involved in substrate binding and catalysis are conserved in AT and StrB1 and are at equivalent topological positions, suggesting a similar reaction mechanism among amidinotransferases. The binding site for L-arginine had been deduced from its complex with AT. Molecular modeling revealed a possible binding mode for the second substrate *scyllo*-inosamine 4-phosphate.

L-Arginine:inosamine-phosphate amidinotransferases catalyze two transamidination reactions in the biosynthesis of the streptomycin family of antibiotics (*1*−*3*; for reviews, see refs *4* and *5*) (Figure 1). These aminoglycoside antibiotics are mainly produced by certain strains of *Streptomyces* sp. and cause translational errors and inhibition of translocation of the growing polypeptide chain by binding to the 30S ribosomal A-site 16S rRNA (*6*, *7*). Streptomycin biosynthesis is regulated by A-factor [2-isocapryloyl-3*R*-(hydroxymethyl)-γ-butyrolactone] (*8*−*10*) which induces the transcription of *str*R, a transcriptional activator of streptomycin biosynthesis genes such as *str*B1 (*11*−*16*).

The substrate specificity of inosamine-phosphate amidinotransferases is rather broad. The physiological amidino donor for the transamidination reaction is L-arginine, but L-canavanine (the guanidinoxy analogue of arginine), streptidine 6-phosphate (compound 4 in Figure 1), 2-deoxystreptidine-6-phosphate, and *N*-amidino-*scyllo*-inosamine 4-phos-

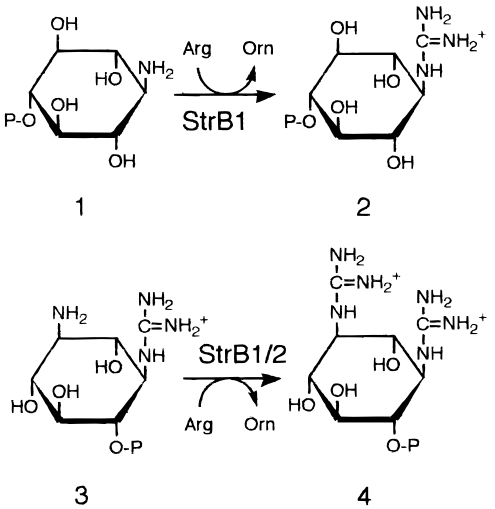

FIGURE 1: Role of amidinotransferases in the biosynthesis of the aminoglycosid antibiotics streptomycin and bluensomycin (*2*, *3*; for reviews, see refs *4*, and *5*). *S. griseus* and *S. glaucescens* possess two amidinotransferases, which convert *scyllo*-inosamine 4-phosphate (compound **1**) into *N*-amidino-*scyllo*-inosamine 4-phosphate (**2**) and N^1-amidinostreptamine 6-phosphate (**3**) into streptidine 6-phosphate (**4**). Whether only one amidinotransferase (StrB1) can carry out both transamidination steps is controversial (see the introductory section).

‡ The coordinates of the StrB1 structure have been deposited with the Brookhaven Protein Data Bank (file name 1bwd) and will be released immediately.

* Corresponding author. Fax: ++49 89 85783516. Phone: ++49 89 85782660.

§ Max-Planck-Institut für Biochemie.

|| Bergische Universität GH.

10.1021/bi981949p CCC: $15.00
Published on Web 11/26/1998

phate (weak donor, compound **2**) can also serve as amidino donors in vitro. The physiological amidino acceptors are *scyllo*-inosamine 4-phosphate (compound **1**) and N^1-amidinostreptamine 6-phosphate (compound **3**), but other known acceptors include 3-amino-3-deoxy-*scyllo*-inosamine 4-phosphate and its 2-deoxy derivative, 2-amino-2-deoxy-*neo*-inositol 5-phosphate, L-ornithine, L-canaline (the aminoxy analogue of ornithine), glycylglycine, 1,4-diaminobutyl-1-phosphonate, and hydroxylamine (*1*).

It is a matter of controversy whether one or two amidinotransferases catalyze the two nonconsecutive transamidinations in *Streptomyces griseus* and *Streptomyces glaucescens*. The two L-arginine:inosamine-phosphate amidinotransferases (StrB1[1] and StrB2) of these organisms are 69 and 61% identical, respectively (*4*). However, it is not clear to date whether only StrB1 or both amidinotransferases are active toward the physiological substrates *scyllo*-inosamine 4-phosphate, N^1-amidinostreptamine 6-phosphate, or both (Figure 1). Pla (*17*) reported the purification of two different amidinotransferase activities, whereas all other studies could only detect one active enzyme species (*3*, *18*, *19*) or showed that StrB1 can catalyze both transamidination reactions (*3*, *19*, *20*). So far, attempts to measure StrB2 activity have failed (*21*), and it is notable that the nucleophilic cysteine which is the key residue for amidine transfer by human L-arginine:glycine amidinotransferase (AT) (*22*−*24*) is not conserved but replaced by a glycine residue in StrB2 from *S. griseus*.

Active StrB1 from *S. griseus* was recombinantly expressed as a six-histidine fusion protein in *Escherichia coli* and purified by nickel nitrilotriacetate−agarose affinity chromatography. Native StrB1 consists of 348 amino acids corresponding to a calculated molecular mass of 38.67 kDa and is a monomer in solution (*3*). Amidinotransferase StrB1 from *S. griseus* shares 39% amino acid sequence identity and 48% homology with AT whose crystal structure has been solved previously to 1.9 Å (*24*).

In this work, we describe the crystal structure of the StrB1 amidinotransferase from *S. griseus* at 3.1 Å resolution, the first structure of a bacterial amidinotransferase, and compare it with AT.

EXPERIMENTAL PROCEDURES

Construction of the Expression Plasmid. For inducible and strong recombinant expression, the gene encoding L-arginine:inosamine-phosphate amidinotransferase StrB1 from *S. griseus* (StrB1) was amplified from the plasmid pCH17.1 (provided by W. Piepersberg) and put under the control of a T7 polymerase/promotor system. DNA sequencing of plasmid pCH17.1 revealed that the C-terminal sequence is not TARETYQF as found in the EMBL database (accession no. S55493/Y00459) but TGALETYQF, leading to a C-terminal sequence more similar to those of other bacterial or mammalian amidinotransferases. The obtained sequences were used to synthesize a 5′-primer including an N-terminal factor X_a-cleavage site (IEGR), an *Eco*RI cleavage site (5′-TAT CGT GAA TTC ATC GAG GGT AGA AGC CTT GTA AGC GTC CAC AAC GAA TGG G-3′), and a 3′-primer including an *Eco*RI cleavage site and two stop codons (5′-CGA ATC GAA TTC TCA TCA GAA CTG GTA CGT CTC-3′). The region encoding StrB1 was amplified by PCR, and the generated 1070 bp fragment was digested with *Eco*RI and subsequently inserted into the *Eco*RI cloning site of vector pRSETHE, a pRSETAT38H derivative (*23*) where the coding sequence for L-arginine:glycine amidinotransferase (AT) was excised and the *Bam*HI restriction site was mutated into an *Eco*RI site. The correctness of the resulting expression vector pRSET-StrB1 was verified by sequencing the whole insert in both directions. The 24 bp between the ATG start codon and the *Eco*RI restriction site, the *Eco*RI site, and the factor X_a-cleavage site extend the length of the recombinant protein from 348 to 361 amino acids and encode amino acids MAHHHHHHGSIEGR′SLV..., where the sequence SLV comprises the first amino acids of the StrB1 protein (without the N-terminal methionine).

Expression and Purification. The expression and purification of recombinant StrB1 by nitrilotriacetate−agarose affinity chromatography were carried out as described previously (*23*) with 1 mM glutathione present in all chromatographic steps. The washing step was carried out with 50 mM imidazole in washing buffer [50 mM sodium phosphate buffer (pH 6.2), 300 mM NaCl, and 1 mM glutathione] since the StrB1 amidinotransferase eluted at about 100 mM imidazole in washing buffer and the protein was dialyzed two times against 5 L of 50 mM Tris-HCl (pH 7.8), 1 mM glutathione, and 0.2 mM EDTA. About 0.5−1 mg of 90−95% pure StrB1 protein per liter of expression culture was obtained. The purification was monitored by SDS−PAGE (*25*). The protein concentration was determined spectrophotometrically using a specific absorption coefficient at 280 nm of 1.46 cm^2 mg^{-1}. The protein was characterized by N-terminal sequencing, ESI-MS, and enzymatic activity. The deconvoluted ESI-MS spectrum revealed a major peak at 40 170 Da compared to the calculated mass of 40 163 Da. The specific activity was 0.6 μmol mg^{-1} h^{-1} using L-arginine and hydroxylamine as the amidine donor and acceptor, respectively (*26*).

Crystallization. Recombinant StrB1 with an N-terminal histidine tag was crystallized at 20 °C using the hanging drop method. The droplets were made from 2 μL of a protein solution (7.3 mg/mL) in 50 mM Tris-HCl (pH 7.8), 1 mM glutathione, 0.2 mM EDTA, and 2 μL of a reservoir solution containing 20% (w/v) PEG 4000, 0.1 M sodium citrate buffer (pH 5.0), and 0.2 M ammonium acetate and equilibrated against the reservoir solution. Tetragonal-bipyramidal shaped crystals of approximately 0.1 mm appeared after 4 weeks. The crystals belonged to the tetragonal space group $P4_3$ with the following cell constants: $a = b = 121.30$ Å, $c = 63.74$ Å (Table 1). The asymmetric unit contained two molecules with a solvent content of 58% ($V_m = 2.92$ Å^3/Da) (*27*).

Data Collection and Processing. X-ray data were collected on a MAR Research imaging plate detector system at 18 °C mounted on a Rigaku RU200 rotating anode X-ray generator with CuKα radiation at a λ of 1.542 Å. Images were processed with MOSFLM (*28*), and data were scaled and reduced using ROTAVATA/AGROVATA/TRUNCATE (*29*).

[1] Abbreviations: AT, human mitochondrial L-arginine:glycine amidinotransferase; EDTA, ethylenediaminetetraacetic acid; ESI-MS, electrospray ionization mass spectrometry; IPTG, isopropyl β-D-thiogalactopyranoside; ncs, noncrystallographic symmetry; PEG, poly(ethylene glycol); rms, root-mean-square; SDS−PAGE, sodium dodecyl sulfate−polyacrylamide gel electrophoresis; StrB1, L-arginine:inosamine-phosphate amidinotransferase from *S. griseus*.

Table 1: Data Collection and Refinement Statistics

Data Collection	
space group	$P4_3$
cell axis, *a* and *b*, *c* (Å)	121.30, 63.74
resolution (Å)	3.1
total observations [$I > 2\sigma(I)$]	37728
no. of unique reflections	14273
completeness (%)	
∞−3.10 Å	85.6
3.21−3.10 Å	75.3
R_{merge} (%)[a]	
∞−3.10 Å	14.4
3.21−3.10 Å	34.5
Refinement	
resolution range in refinement (Å)	10.0−3.1
no. of reflections used for refinement	12488
no. of non-hydrogen atoms per asymmetric unit	5456
R-factor (%)[b]	19.7
free *R*-factor (%)[c]	26.5
rmsd from ideal geometry	
bond lengths (Å)	0.009
bond angles (deg)	2.3
rmsd of bonded *B*-factors (Å^2)	1.35
mean *B*-value protein (Å^2)	21.3
rmsd between molecules A and B (C_α) (Å)	0.038

[a] $R_{merge} = \sum_h\sum_i|I(h, i) - \langle I(h)\rangle|/\sum_h\sum_i I(h, i)$, were $I(h, i)$ is the intensity value of the *i*th measurement of *h* and $\langle I(h)\rangle$ is the corresponding mean value of *h* for all *i* measurements of *h*; the summation is over all measurements. [b] *R*-factor $= \sum|F_o - F_c|/\sum F_o$, where F_o is the observed and F_c the calculated structure factor amplitude. [c] The free *R*-factor was calculated by randomly setting aside 10% of the observed reflections.

The statistics of data collection and refinement are given in Table 1.

Molecular Replacement. The structure of StrB1 amidinotransferase was solved by Patterson search techniques using the program AMoRe (*30*). A modified AT model lacking amino acids 224−245 (human amidinotransferase numbering; *23*) and alanine in nonidentical positions except for glycine was used as a search model. The Patterson search was performed from 15 to 5 Å using the phased translation function in the translational search. The solution showed two highest peaks in the rotation and translation function corresponding to both monomers, and after final rigid-body fitting, the correlation factor was 48.2 with an *R*-factor of 40.5%.

Model Building and Refinement. The coordinates of both correctly oriented monomers A and B were subjected to rigid-body refinement using X-PLOR (*31*) with each molecule divided into two domains (residues 64−223 and 246−423 of the AT model). Refinement using the parameter set of Engh and Huber (*32*) and cyclic *ncs* averaging with MAIN (*33*) ($R_{back,initial} = 16.6\%$) yielded an interpretable electron density map. The atomic model was built with the program ESV-FRODO (*34*) on an ESV-30 graphic workstation. Many cycles of model building and crystallographic refinement, including simulated annealing with a starting temperature of 4000 K, Powell energy minimization followed by overall B-factor refinement using data between 8.0 and 3.1 Å, and *ncs* averaging ($R_{back,final} = 11.2\%$) were carried out. Step by step, the loop connecting the two segments of residues 64−223 and 246−423 of the initial search model and the sequence of StrB1 was fitted to the electron density. The AB dimer was generated from the B monomer by applying the symmetry operator relating the two monomers in the asymmetric unit using MAIN (*33*). Some additional rounds of refinement with REFMAC using data from 10.0 to 3.1 Å, applying bulk solvent correction, tight ncs positional restraints, and individual but highly restrained *B*-factor refinement, resulted in a final *R*-factor of 19.7% (free *R*-factor 26.5%).

Quality of the Final X-ray Model. The final model of StrB1 comprises monomers A and B each with residues 1−348. Solvent molecules were not included. The quality of the final model is summarized in Table 1. Arg1 is the last amino acid of the N-terminal tag and therefore substitutes for the N-terminal methionine of the wild-type protein. The hexahistidine tag and the factor X_a-cleavage site are not visible in the electron density map. The side chains which appear to be disordered (R1, K59, H66, K92, D159, Q164, K204, D212, K221, R257, D275, K276, R306, and K310) are located mainly on the protein surface and were excluded from phasing. The tight ncs positional restraints resulted in almost identical monomers A and B with an rms deviation of C_α-positions of 0.038 Å. The Ramachandran plot (*36*) calculated with the program PROCHECK (*37*) shows that 82.1% of the non-glycine and non-proline residues are located in most favored regions, 17.6% in additional allowed regions, and only Ser144 is located in generously allowed regions of (ϕ, and ψ) values. The mean coordinate error estimated from a Luzzati plot (*38*) is 0.46 Å.

Modeling Experiments. Modeling experiments were carried out with FlexX (*39*), and multiple ring conformations of the inositol moiety were taken into account using CORINA (*40*). The ligands were built with SYBYL (*41*), and the active site was defined by manually placing a ligand into the active site of StrB1.

RESULTS AND DISCUSSION

Molecular Structure. The L-arginine:inosamine-phosphate amidinotransferase StrB1 from *S. griseus* (StrB1) amidinotransferase consists of five $\beta\beta\alpha\beta$-modules in cyclic arrangement generating a pseudo-5-fold symmetric particle with dimensions of 50 Å × 45 Å × 40 Å (Figure 2). Each $\beta\beta\alpha\beta$-module is built up from a three-stranded mixed β-sheet with considerable variations in the length of the strands in the connecting segments. The strand directions follow roughly the particle pseudo-5-fold axis. The first strand occupies the innermost position, while the following two parallel β-strands are further away from the central axis (Figure 2a). The first module has only the two outer β-strands (S1 and S2), but the β-sheet is completed by an extra strand S15 of module V (Figure 2a). The connectivity in the mixed β-sheets is described by +1, +1*x* (*42*), where the inner strand makes a hairpin connection to the middle strand which in turn is linked to the outer strand via a right-handed crossover connection containing an insertion helix. The connecting segments that complete the individual $\beta\beta\alpha\beta$-modules are poor in secondary structure elements and contain mainly short turn-forming 3_{10}-helices resulting in a high content of turn and coils of 56% compared to a content of 26 and 18% for helices and β-sheets, respectively. Comparison with the crystal structure of human L-arginine:glycine amidinotransferase (AT) (*24*) revealed a similar fold with an almost complete conservation of the secondary structure elements (Figure 3) but with large conformational rearrangements in loops around the active site (see below).

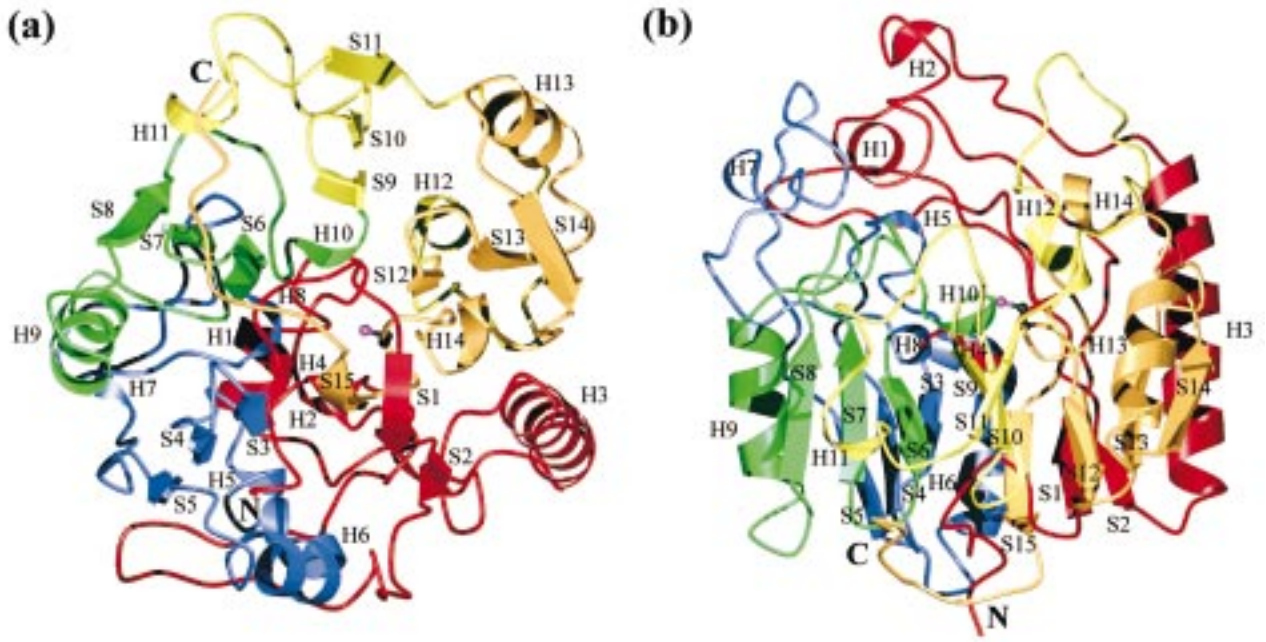

FIGURE 2: Ribbon plot of the StrB1 structure. The individual modules are colored as follows: red (module I, residues 1−109), blue (module II, residues 110−182), green (module III, residues 183−231), yellow (module IV, residues 232−287), and orange (module V, residues 288−348). (a) View from the bottom down the pseudo-5-fold axis. Five $\beta\beta\alpha\beta$-modules are arranged circularly around a pseudo-5-fold axis. The putative active site cysteine residue 332 is shown in a ball-and-stick representation. (b) Side view of StrB1. The secondary structure elements were determined with DSSP (*44*), and the figure was produced with MOLSCRIPT (*45*) and rendered with POV-Ray.

StrB1 Dimer. The asymmetric unit contains two molecules of StrB1 which are related by a local 2-fold symmetry axis roughly parallel to the pseudo-5-fold axis. The dimer interface is rather planar and similar to that of AT. It is formed by predominantly hydrophobic residues in the region between H5 and H8 of module II and from residues in helix H9 of module III. For both StrB1 and AT, size exclusion chromatography had suggested a monomeric state in solution (*3*), whereas sedimentation equilibrium experiments (unpublished results for StrB1; *43*) and the crystallographic data show that StrB1 and AT form dimers (*24*).

Comparison with Human L*-Arginine*:*Glycine Amidinotransferase* (*AT*). StrB1 from *S. griseus* shares between 54% (*S. glaucescens* StrB2) and 86% (*Streptomyces galbus* StrB1) sequence identity with other bacterial amidinotransferases and shares 39% sequence identity with AT (Figure 3). The overall fold of StrB1 is similar to that of AT. The rms deviations between the StrB1 and AT modules are as follows: 3.3 Å (module I, calculated for 107 equivalent C_α-atoms), 1.8 Å (module II, 73 C_α-atoms, calculated without residues 228−240 of AT), 1.6 Å (module III, 49 C_α-atoms), 3.4 Å (module IV; 55 C_α-atoms), and 1.2 Å (module V, 61 C_α-atoms) [MAIN (*33*)]. However, five regions are found in significantly different conformations. These regions include the 40-loop (Pro27−Ala52), the 170-loop (Ala162−Glu169), the 220-loop (Cys219−Thr226), the 250-loop (Val247−Asn261), and the 270-loop (Asp269−Cys279) (Figure 4). Three of these loops (the 40-loop, the 170-loop, and the 270-loop) are located at the top of the molecule and are involved in the formation of the active site entrance, whereas the other two loops (the 220-loop and the 250-loop) lead from the active site to the side of the molecule (Figure 4). In contrast to that of AT, the arrangement of loops around the active site creates a comparatively wide and solvent-exposed depression in the surface of the molecule compared to the narrow active site channel in AT (Figure 5). The architecture of the active site of StrB1 in comparison to AT may be best explained starting with the 170-loop. The deletion of helix H9 in AT results in a reorganized polypeptide chain consisting of two tight turns (Figure 6). This opens the active site entrance and creates some extra space that is partly compensated for by a movement of the neighboring 40-loop toward the 170-loop. The fold of the 40-loop differs greatly from the corresponding region in AT affecting both the active site entrance and the interior of the cavity. For example Tyr38 is completely buried in the 40-loop, whereas the corresponding Tyr100 of AT is swung over the active site like a lid and shields the active site channel [residues of glycine amidinotransferase (AT) are distinguished from those of StrB1 by the suffix AT] (Figure 6). Residue Glu37 of StrB1 extends into the cavity and increases its acidic character, whereas in AT, residue Asn98 is located in the south rim (refers to the standard orientation of Figure 6) and projects toward the active site entrance. The displacement of the 40-loop in the southeast of the active site also induces a concomitant reorganization of the 270-loop in the south. This loop moves toward the 40-loop to which it is linked by a salt bridge between $N^{\epsilon 2}$ of His278 and the carboxylate oxygen $O^{\epsilon 2}$ of Glu37 (3.0 Å). Substrate binding residue Cys279 moves back by ≈2.5 Å. The 270-loop is fastened to the amidino group of Arg324 by hydrogen bonds from the carboxylate group of Asp269 and by the carbonyl oxygen of Cys279 (2.9 and 2.7 Å), leading to a concomitant local distortion of the segment from residue Thr321 to Thr325.

The other two segments that adopt a different conformation in comparison to AT lead from the active site to the side of the molecule and comprise the 220- and 250-loops (Figure 4). The distortion of the 250-loop does not change the spatial position of substrate binding residue Arg246 at the N-terminal end of the 250-loop. The conformation of the 220-

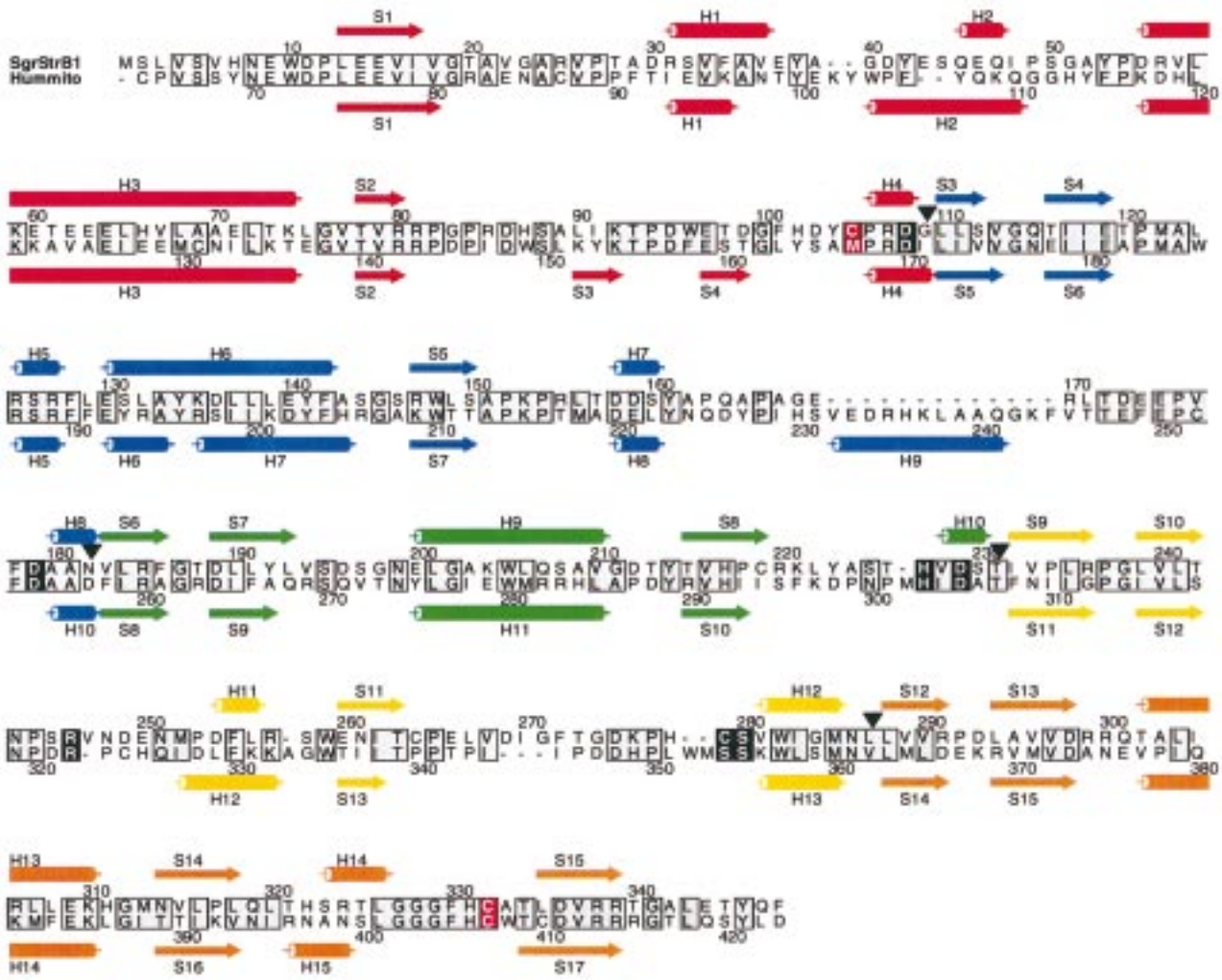

FIGURE 3: *S. griseus* StrB1 and AT secondary structure and sequence alignment. The secondary structure elements of both AT and StrB1 belonging to modules I−V are red, blue, green, yellow, and orange, respectively. For StrB1, the short antiparallel β-sheet S3/S4 of human mitochondrial amidinotransferase is not assigned by DSSP (*44*), but it is assigned by RASMOL (*46*) and STRIDE (*47*). The first five residues of helix H6 and helix H12 are in a 3_{10}-conformation. The most abundant amino acid for each position is shown against a yellow background. Residues implicated in substrate binding or catalysis are shown against a gray background. The two cysteine residues found in the active site of StrB1 are shown on a red background. The module boundaries are indicated by black triangles. The AT sequence starts with the first amino acid observed in the crystal structure (*24*). Human mitochondrial AT is synthesized as a 423-amino acid preprotein and is cleaved by a signal peptidase after residue 37 to generate the mature protein. The numbering of the StrB1 and human mitochondrial sequences both start with the N-terminal methionine. The C-terminal sequence GALETYQF of the crystallized StrB1 protein from *S. griseus* is shown. Hummito represents human mitochondrial amidinotransferase [PDB ID code 1JDW, EMBL accession number (Ac) S68805]; SgrStrB1, represents *S. griseus* StrB1 (Ac S55493, Y00459). The sequences were aligned using the GCG package (*48*) and formated with ALSCRIPT (*49*).

loop (Cys219−Thr226) is significantly different from that of AT, whereas the preceding catalytic residues His227 and Asp229 are observed in similar spatial positions (Figure 4). This region corresponds to the flexible 300-flap of AT, which moves in concert with helix H9 upon substrate binding (*24*). This ligand-induced fit mechanism leads to a closed and an open conformation. StrB1 contains a single amino acid deletion in this region, resulting in a conformation which is different from both the closed and open AT conformations. In particular, $Asn300^{AT}$ and $Met302^{AT}$ are topologicaly replaced by Ala224 and Thr226 in StrB1, enlarging the active site compartment. Residue $Asn300^{AT}$ is suggested to play a key role in the ligand-induced movements, because it sterically interferes with the carboxylate and α-amino group of the substrate L-arginine upon binding, inducing the aforementioned conformational changes. This residue is replaced by an alanine residue in StrB1, suggesting that StrB1 does not switch between an open and closed state.

A comparison of the electrostatic solid surface representation of StrB1 with that of AT illustrates the striking enlargement of the active site (Figure 5). The inner wall of the cavity is lined by many positively (H102, R170, R127, H227, R246, and H278) and negatively charged residues (E37, D41, D108, D179, D196, and D229) with a preponderance of anionic residues. Since the conformational differences are mainly entrance-restricted, the surface charge distributions look different when viewed down the active site, but look similar when viewed from the opposite side. Three features of the surface of StrB1 in comparison to AT are notable: a prominent anionic patch at the far southeast of the active site entrance with a clustering of Glu169, Asp173, Glu174, and Glu200; the lack of a helix corresponding to the AT helix H9, which changes the shape of the southeast rim and removes two acidic solvent-exposed residues

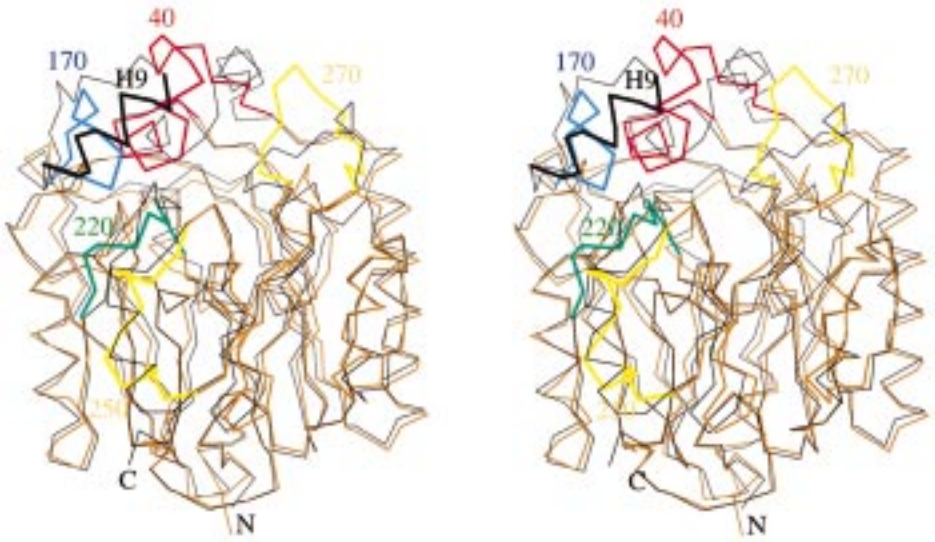

FIGURE 4: Superimposition of the C_α-traces of StrB1 (brown) and AT (black). The orientation is the same as in Figure 2b. The loops of StrB1 which deviate most from AT (i.e., the 40-, 170-, 220-, 250-, and 270-loop) are highlighted by bold lines in the colors of the corresponding modules as in Figure 2. Helix H9 of AT, which is deleted in StrB1, is bold and black. The figure was prepared using MOLSCRIPT (*45*).

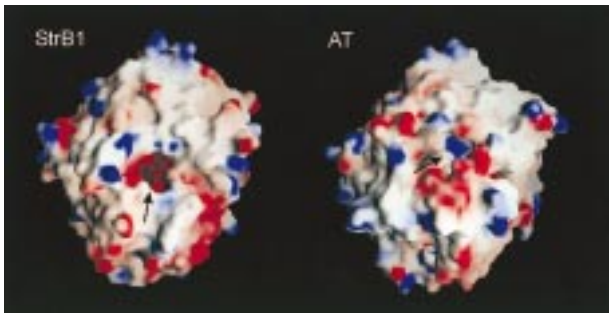

FIGURE 5: Comparison of the electrostatic surface potential of StrB1 amidinotransferase (left) with AT (right). The view is down the active site. The difference in active site architecture with the open active site cavity of StrB1 in comparison to the very narrow active site channel of AT is easily seen. The active site entrances are indicated by arrows. The figure was produced with GRASP (*50*).

FIGURE 6: Superimposition of loops around the active site of StrB1 (yellow) and AT (light blue). The major structural differences occur at the active site entrance and involve the 270-loop in the west, the 40-loop in the southeast, and the 170-loop in the east. In addition, catalytic residues Arg322 and Cys322 are shown. The deletion of helix H9 of AT results in a reorganized 170-loop and may cause the observed conformation of the 40-loop and the 270-loop. In comparison to AT, the active site of StrB1 is wide open and solvent-exposed. The labeled residues are discussed in the text. The figure was produced with SETOR (*51*).

(Glu233 and Asp234); and a rather planar and hydrophobic patch corresponding to the dimer interface in the north hemisphere of the molecule, when rotated 180° on the horizontal axis (not shown). Generally, StrB1 contains more acidic and less basic residues than AT, resulting in a significantly different calculated p*I* value of 4.9 compared to 8.0.

Substrate Binding Sites. The active site topology of StrB1 is similar to that of AT, and almost all active site residues are conserved (Figure 7). However, the carbonyl oxygen of Thr226 and the side chain of Asp229 were fitted to the electron density in a different conformation than in AT. The electron density is not so well defined as to exclude an AT-like conformation at these locations. The arginine binding site was deduced from the structure of AT in complex with L-arginine (*24*). In that structure, the interactions include four hydrogen bonds from Ser280 N and from Cys279 S^γ and Ser280 O^γ to the carboxylate group and from His227 $N^{\delta 1}$ to the ϵ-imino group of the bound L-arginine. Three salt bridges are formed from Arg246 to the carboxylate group and from Asp108 and Asp229 to the guanidino group. If this binding mode is assumed, the nucleophilic Cys332 and Asp229 would come far too close (<2 Å) to the guanidino group of the bound L-arginine in StrB1. However, a rearrangement of Asp229 into a conformation similar to that of AT would lead to reasonable hydrogen bond distances to the substrates. Residues Asn286 and Asp179 are not directly involved in substrate binding, but Asn286 may be involved in the activation of the nucleophilic cysteine (*24*) and Asp179 in stabilizing the imidazole ring of His227, which acts as a general acid and/or base (*22*).

The binding mode of the second substrate *scyllo*-inosamine 4-phosphate (Figure 1) was predicted by docking experiments using FlexX (*39*). We assumed the enzyme was rigid, whereas the multiple flexible ring conformations of the

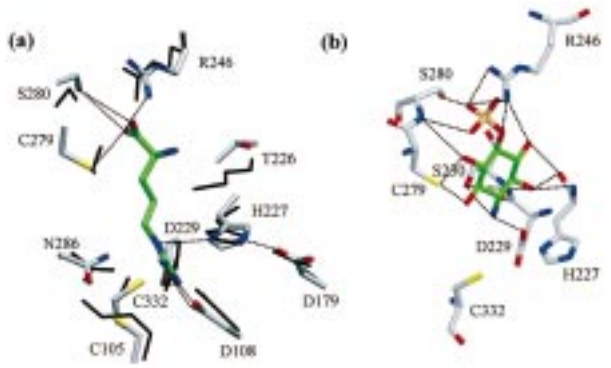

FIGURE 7: Binding modes of L-arginine and of inosamine phosphate. (a) Superimposition of the active sites of StrB1 (yellow) and AT (green). The proposed L-arginine binding site was deduced from its known complex with AT. (b) The proposed inosamine phosphate binding site of StrB1. A modeled *scyllo*-inosamine 4-phosphate (green) is involved in numerous hydrogen bonds (dashed lines) with residues of StrB1. The residues of StrB1 are labeled. The figure was produced with SETOR (*51*).

inositol moiety of the ligand were taken into account using CORINA (*40*). However, initial docking trials gave a clear solution only when an enzyme model with a different side chain conformation of Asp229 was used. The best placement yielded a free energy value of -37.4 kJ mol^{-1} compared to -24.7 kJ mol^{-1} for the second solution corresponding to a 165-fold tighter binding. The ring of *scyllo*-inosamine 4-phosphate is found in an ideal low-energy chair conformation with all substituents in equatorial positions and is predicted to be involved in numerous interactions with active site residues (Figure 7b).

As mentioned in the introductory section, *S. griseus* and *S. glaucescens* possess two related L-arginine:inosamine-phosphate amidinotransferases (StrB1 and StrB2) with 69 and 61% amino acid identity. Remarkably, the catalytic cysteine residue 332 is mutated in the StrB2 proteins from both strains. This finding brought to light the question of whether another cysteine residue could substitute for the nucleophilic Cys332. Indeed, a second cysteine residue (Cys105) was observed in the active site of StrB1. Cys105 is only ≈4 Å from the catalytic Cys332 and occurs as a free thiol. However, if the ion pair formation between the substrates and Arg246 is considered a key step in catalysis, the substrates are too short to reach Cys105. This is in accordance with the fact that an enzymatic activity for *S. griseus* StrB2 could not be shown (*21*). Therefore, active StrB2 would require a completely different active site topology and/or reaction mechanism.

Proposed Reaction Mechanism. The conserved active site geometry suggests a similar mechanism for transamidination of StrB1 and AT (Figure 8). In analogy to catalysis by AT (*22*), the proposed transamidination starts with the binding of L-arginine and the subsequent nucleophilic attack of the

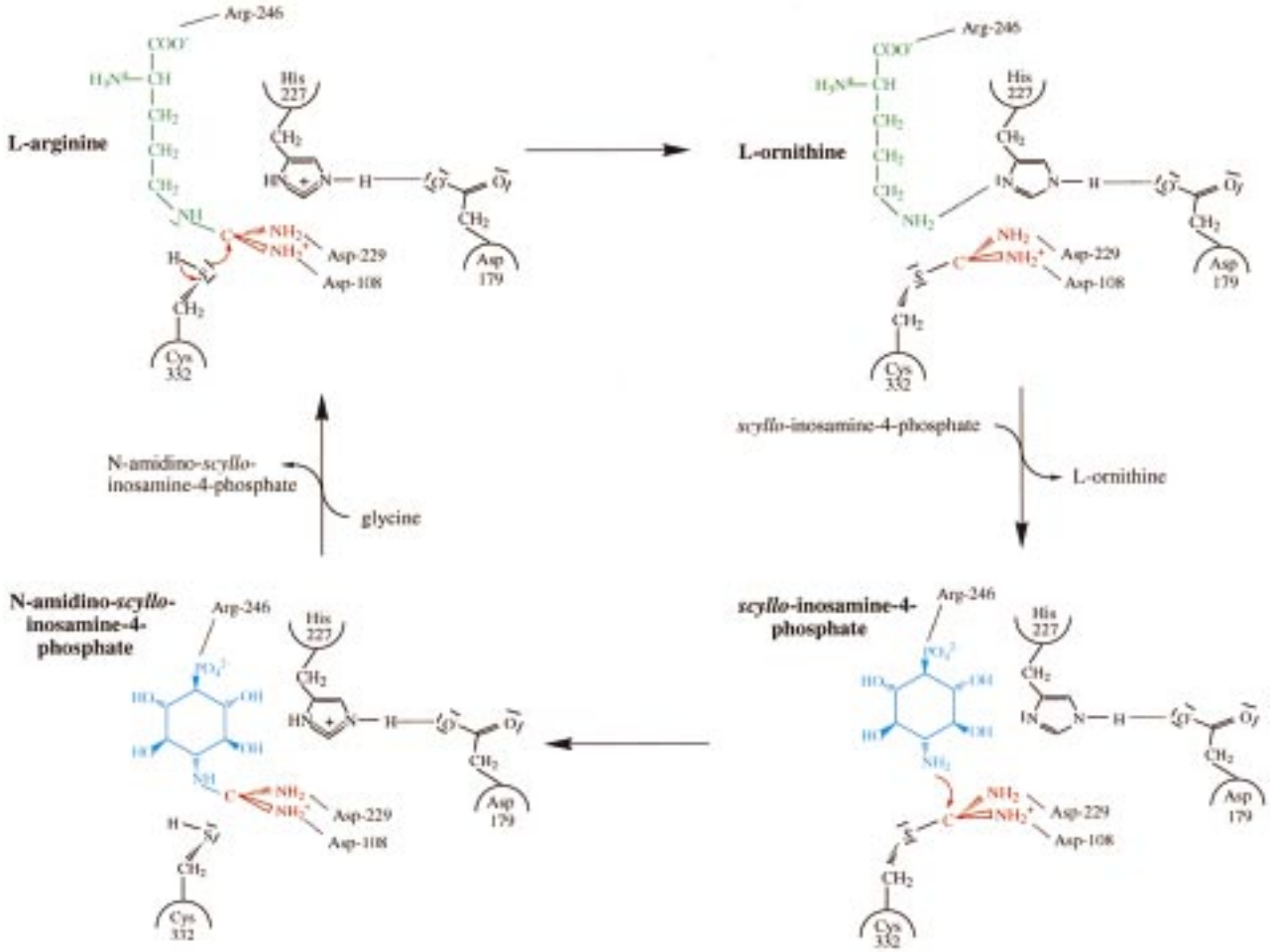

FIGURE 8: Proposed reaction mechanism of StrB1. From the substrate binding residues, only Arg246, Asp108, and Asp229 are shown. The transamidination involves the transient attachment of an amidino group to Cys332.

thiolate anion of Cys332 on the positively polarized carbon atom of the guanidino group. As the tetrahedral transition state decays, a covalent cysteine−amidino intermediate and L-ornithine are formed. The binding of the amidino acceptor *scyllo*-inosamine 4-phosphate, the nucleophilic attack on the planar isothiourea group, and the liberation of the reaction product are the final steps of the reaction cycle. However, a detailed picture of thiol activation and deprotonation−reprotonation of the substrates and products is still missing. The deprotonation of the thiol group of Cys332 as a prerequisite for the nucleophilic attack must occur in the acidic environment of the carboxyl groups of Asp108 and Asp229 which are only 3.5−4.0 Å away from S^{γ} of Cys332. We suggest a proton transfer pathway from the active site Cys332 to Asp229 and next from Asp229 to $N^{\delta 1}$ of His331. The $N^{\epsilon 2}$ of His331 in turn is hydrogen bonded to Glu9, which increases the pK_a value of His331. An alternative proton transfer pathway might start with the transfer of the thiol proton to Asp108 and next from Asp108 to Arg127 or to His227. All these residues are highly conserved among amidinotransferases. However, the Cys332−Asp108 and Asp108−His227 distances are rather long (around 4 Å).

Substrate Specificity. As mentioned in the introductionory section, amidinotransferases seem to be relatively unspecific. However, the location of the phosphate group relative to the amino group to be transamidinated is critical as seen in Figure 1. The amino substituent to be transamidinated must obviously occupy a position diametrically opposite of the phosphate substituent. These are the 1 and 4 positions of the inositol ring. This $|s_N - s_P| = 3$ rule, where s_N is the position of the amino group to be transamidinated and s_P the position of the phosphate group, also holds for the second transamidination (conversion of compound **3** to **4**, Figure 1), where the phosphate group is at position 6, whereas the amino group is located at position 3. Aminocyclitols with the exocyclic amino and phosphate substituents at neighboring ring carbons such as N^1-amidino-3-amino-3-deoxy-*scyllo*-inosamine 4-phosphate or 3-amino-3-deoxy-*scyllo*-inosamine 4-phosphate cannot be converted (*1*). Another stereochemical condition seems to be the configuration of the stereocenters C(s_N) and C(s_P) resulting in a diequatorial s_N,s_P-inositol ring (Figure 7b). This positional requirement is reflected in the structure by the formation of an ion pair between the phosphate group of the substrates and Arg246 and the orientation of the amino group toward the putative nucleophilic Cys332. However, it is not readily obvious from the structure why 2-amino-2-deoxy-*neo*-inositol 5-phosphate, which differs from *scyllo*-inosamine 4-phosphate in the configuration of all four hydroxyl groups, is an excellent amidino acceptor (*1*). There is evidence from several studies (*3*, *18*, *19*) that StrB1 can carry out both nonconsecutive transamidination reactions in streptomycin biosynthesis. To test this proposal, N^1-amidinostreptamine 6-phosphate (compound **3** in Figure 1) was manually placed into the active site. With a conformation and orientation of the inositol ring similar to those of the modeled *scyllo*-inosamine 4-phosphate, the guanidino group at position 1 would clash with Ser230 and would come too close to the positively charged guanidino group of Arg246, resulting in cationic repulsion. After an ≈180° rotation of the ligand around its C3−C6 axis, the guanidino group points into the spacious active site cavity and is 4.5 Å from the carbonyl oxygen of His278 and 5.5 Å from the side chains of Asp37 and Thr226. However, upon rotation all exocyclic substituents remain in an equatorial position but change their spatial position. Therefore, a tight binding would require alternative ring conformations and/or a different binding mode.

This structure provides a framework for further analysis of the mechanism of transamidination in streptomycin biosynthesis. However, structural and biochemical studies on both StrB1 and StrB2 amidinotransferases are required to explain the problem of substrate specificity with emphasis toward the various inositol phosphate analogues which differ in exocyclic substituents and/or stereochemistry.

ACKNOWLEDGMENT

We thank T. Ploom for help with cyclic averaging and H.-G. Beisel for computational assistance.

REFERENCES

1. Walker, J. (1973) in *The Enzymes* (Boyer, P. D., Ed.) 3rd ed., pp 497−509, Academic Press, New York.
2. Walker, J. B. (1975) *Methods Enzymol. 43*, 451−458.
3. Ohnuki, T., Imanaka, T., and Aiba, S. (1985) *J. Bacteriol. 164*, 85−94.
4. Piepersberg, W. (1997) in *Biotechnology of Antibiotics* (Strohl, W. R., Ed.) pp 81−163, Marcel Dekker, New York.
5. Piepersberg, W., and Distler, J. (1997) in *Biotechnology* (Rehm, H.-J., and Reed, G., Eds.) Vol. 7, pp 397−488, Verlag Chemie, Weinheim, Germany.
6. Fourmy, D., Recht, M. I., Blanchard, S. C., and Puglisi, J. D. (1996) *Science 274*, 1367−1371.
7. Spickler, C., Brunelle, M., and Brakier-Gingras L. (1997) *J. Mol. Biol. 273*, 586−599.
8. Khokhlov, A. S. (1982) in *Overproduction of microbial products* (Krumphanzel, V., Sikyta, B., and Vanek, Z., Eds.) pp 97−109, Academic Press, London.
9. Miyake, K., Horinouchi, S., Yoshida, M., Chiba, N., Mori, K., Nogawa, N., Morikawa, N., and Beppu T. (1989) *J. Bacteriol. 171*, 4298−4302.
10. Miyake, K., Kuzuyama, T., Horinouchi, S., and Beppu, T. (1990) *J. Bacteriol. 172*, 3003−3008.
11. Dodd, I., and Egan, J. B. (1990) *Nucleic Acids Res. 18*, 5019−5026.
12. Vujaklija, D., Ueda, K., Hong, S., Beppu, T., and Horinouchi, S. (1991) *Mol. Gen. Genet. 229*, 119−128.
13. Vujaklija, D., Horinouchi, S., and Beppu, T. (1993) *J. Bacteriol. 175*, 2652−2661.
14. Horinouchi, S., and Beppu, T. (1994) *Mol. Microbiol. 12*, 859−864.
15. Retzlaff, L., and Distler, J. (1995) *Mol. Microbiol. 18*, 151−162.
16. Thamm, S., and Distler, J. (1997) *FEMS Microbiol. Lett. 149*, 265−272.
17. Pla, L. C. (1971) *Biochim. Biophys. Acta 242*, 541−548.
18. Miller, A. L., and Walker, J. B. (1969) *J. Bacteriol. 99*, 401−405.
19. Walker, J. B. (1974) *J. Biol. Chem. 249*, 2397−2404.
20. Walker, M. S., and Walker, J. B. (1967) *Biochim. Biophys. Acta 136*, 272−278.
21. Pissowotzki, K., Mansouri, K., and Piepersberg, W. (1991) *Mol. Gen. Genet. 231*, 113−123.
22. Fritsche, E., Humm, A., and Huber, R. (1997) *Eur. J. Biochem. 247*, 483−490.
23. Humm, A., Fritsche, E., Mann, K., Göhl, M., and Huber, R. (1997) *Biochem. J. 322*, 771−776.
24. Humm, A., Fritsche, E., Steinbacher, S., and Huber, R. (1997) *EMBO J. 16*, 3373−3385.
25. Schägger, H., and von Jagow, G. (1987) *Anal. Biochem. 166*, 368−379.
26. Van Pilsum, J. F., Taylor, D., Zakis, B., and McCormick, P. (1970) *Anal. Biochem. 35*, 277−286.

27. Matthews, B. W. (1968) *J. Mol. Biol. 33*, 491−497.
28. Leslie, A. G. W. (1994) *Mosflm user guide*, version 5.41, MRC Laboratory of Molecular Biology, Cambridge, U.K.
29. Collaborative Computational Project, Number 4 (1994) *Acta Crystallogr. D50*, 760−763.
30. Navaza, J. (1994) *Acta Crystallogr. A50*, 157−163.
31. Brünger, A. T. (1992) *X-PLOR* (*version 3.851*) *Manual*, Yale University Press, New Haven, CT.
32. Engh, R. A., and Huber, R. (1991) *Acta Crystallogr. A47*, 392−400.
33. Turk, D. (1992) Ph.D. Thesis, Technische Universität, München, Germany.
34. Jones, T. A. (1978) *J. Appl. Crystallogr. 11*, 268−272.
35. Murshudov, G. N., Vagin, A. A., and Dodson, E. J. (1997) *Acta Crystallogr. D53*, 240−255.
36. Ramachandran, G. N., and Sasisekharan, V. (1968) *Adv. Protein Chem. 23*, 283−437.
37. Laskowski, R. A., MacArthur, M. W., Moss, D. S., and Thornton, J. M. (1992) *PROCHECK, version 3.3*, Oxford Molecular Ltd., Oxford, England.
38. Luzzati, P. V. (1952) *Acta Crystallogr. 5*, 802−810.
39. Rarey, M., Kramer, B., Lengauer, T., and Klebe, G. (1996) *J. Mol. Biol. 261*, 470−489.
40. Sadowski, J., Schwab, C. H., and Gasteiger, J. (1997) *CORINA program description*, Version 2.1, Computer-Chemie-Centrum, Universität Erlangen, Nürnberg, Germany.
41. TRIPOS Associates, Inc. (1994) *SYBYL molecular modeling software*, version 6.3, St. Louis, MO.
42. Richardson, J. S. (1981) *Adv. Protein Chem. 34*, 167−339.
43. Gross, M. D., Eggen, M. A., Simon, A. M., and Van Pilsum, J. F. (1986) *Arch. Biochem. Biophys. 251*, 747−755.
44. Kabsch, W., and Sander, C. (1983) *Biopolymers 22*, 2577−2637.
45. Kraulis, P. J. (1991) *J. Appl. Crystallogr. 24*, 946−950.
46. Sayle, R. (1995) *RasMol molecular renderer*, version 2.6, Glaxo Research & Development, Middlesex, U.K.
47. Frishman, D., and Argos, P. (1995) *Proteins*: *Struct., Funct., Genet. 23*, 566−579.
48. Genetics Computer Group (1997) *Wisconsin Package*, version 9.1, Madison, WI.
49. Barton, G. J. (1993) *Protein Eng. 6*, 37−40.
50. Nicholls, A., Bharadwaj, R., and Honig, B. (1993) *Biophys. J. 64*, A166.
51. Evans, S. V. (1993) *J. Mol. Graphics 11*, 134−138.

BI981949P